Available online at www.sciencedirect.com

SCIENCE DIRECT®

Thin Solid Films 469–470 (2004) 274–281

thin solid films

www.elsevier.com/locate/tsf

Corrosion resistance of ZrN_xO_y thin films obtained by rf reactive magnetron sputtering

E. Ariza[a,b], L.A. Rocha[a,b,*], F. Vaz[c], L. Cunha[d], S.C. Ferreira[a], P. Carvalho[c], L. Rebouta[c], E. Alves[e], Ph. Goudeau[f], J.P. Rivière[f]

[a]*Research Centre on Interfaces and Surface Performance, Azurém, 4800-058 Guimarães, Portugal*
[b]*Universidade do Minho, Dept. Eng. Mecânica, Azurém, 4800-058 Guimarães, Portugal*
[c]*Universidade do Minho, Dept. Física, Azurém, 4800-058 Guimarães, Portugal*
[d]*Universidade do Minho, Dept. Física, Campus de Gualtar, 4710-057 Braga, Portugal*
[e]*ITN, Departamento de Física, E.N.10, 2685 Sacavém, Portugal*
[f]*Laboratoire de Métallurgie Physique, Université de Poitiers, 86960 Futuroscope, France*

Available online 18 October 2004

Abstract

The main aim of this work is the investigation of the corrosion resistance of single layered zirconium oxynitride, ZrN_xO_y, thin films in artificial sweat solution at ambient temperature. The films were produced by rf reactive magnetron sputtering, using a pure Zr target at a constant temperature of 300 °C. Two different sets of samples were produced. In the first set of films, the substrate bias voltage was the main variable, whereas in the second set, the flow rate of reactive gases (oxygen/nitrogen ratio) was varied. The control of the amount of oxygen allowed the film properties to be tailored from those of covalent zirconium nitride to those of the correspondent ionic oxide. The corrosion behaviour was evaluated by potentiodynamic polarization and Electrochemical Impedance Spectroscopy (EIS) tests. The analysis of EIS data provided detailed information of the corrosion processes occurring at the surface of the system throughout the immersion time. The modifications of the coating microstructure and/or chemical composition induced by the variation of the deposition parameters were also evaluated and correlated with the corrosion mechanisms occurring in each system.

Keywords: Corrosion; Magnetron sputtering; Thin films

1. Introduction

In the last few years, an emergent field of research is gaining more and more importance—the so-called decorative thin films. These colored films possess a high potential for being applied in high-quality consumer products, such as eyeglass frames, wristwatch casings and wristbands. In fact, while enhancing the appearance of the pieces by lending attractive colorations to their surfaces, these films are supposed to provide simultaneously scratch-resistance and improved corrosion resistance.

Up to now, decorative films are mostly based on elemental materials and also binary nitrides (TiN, golden yellow; ZrN, greenish yellow; HfN, pale greenish yellow [1]) or titanium carbonitrides [1,2]. The color tones attainable are, however, largely restricted to these golden yellows, various shades of grey and black [2,3], although some attempts have been made in order to obtain other colors, based on borides [3]. Recently, a new class of materials is gaining importance for these decorative applications, the so-called metal oxynitrides, MeN_xO_y (Me=early transition metal) [4–6]. This importance results from the fact that the presence of oxygen allows the tailoring of film properties between those of "pure" covalent metal nitride and those of the correspondent largely ionic oxides. Recent publications suggest that the performance of these oxynitrides depends not only on the deposition

* Corresponding author. Universidade do Minho, Dept. Eng. Mecânica, Azurém, 4800-058 Guimarães, Portugal. Tel.: +351 253 510 231; fax: +351 253 516 007.
E-mail address: lrocha@dem.uminho.pt (L.A. Rocha).

0040-6090/$ - see front matter © 2004 Elsevier B.V. All rights reserved.
doi:10.1016/j.tsf.2004.08.091

method but also on both the concentration and distribution of the nitrogen atoms incorporated into the matrix [4–9].

Despite the huge amount of published scientific work on thin films of metallic nitrides and oxides over the last 20 years [10], the area of metal oxynitrides is poorly explored so far and the understanding of the fundamental mechanism that explains both structural and mechanical behaviour is yet insufficient. Also, researches on the corrosion behaviour and on the degradation mechanisms occurring in these films when they are in contact with aggressive environments are missing. In this work, the corrosion behaviour of colored ZrN_xO_y films in contact with artificial sweat solutions is investigated. Particular focus is given to the study of corrosion mechanisms associated to each particular coating system.

2. Experimental details

The ZrN_xO_y samples were deposited by reactive rf magnetron sputtering from a high purity Zr target onto polished high-speed steel (AISI M2). Substrates were ultrasonically cleaned and sputter etched for 15 min in a 0.4 Pa Ar atmosphere (200 W rf power). Depositions were carried out under an Ar/N_2+O_2 atmosphere in an Alcatel SCM650 apparatus, and the substrates were rotating at 60 mm over the target at a constant speed of 4 rpm. The base pressure in the deposition chamber was about 10^{-4} Pa and rose to values around 4×10^{-1} Pa during depositions. A pure zirconium adhesion layer with a thickness of about 0.30 μm was deposited in each sample to improve adhesion. Films were prepared with variation of the gas mixture flux (N_2+O_2), using a constant value of temperature (300 °C) and bias voltage ranging from −75 V to ground state. Reactive gases (N_2+O_2) flux varied from 3.3 to 6.3 sccm, with a partial pressure ranging from 0.02 to 0.05 Pa. The working gas flow (argon) was kept constant at 100 sccm.

The atomic composition of the samples was measured by Rutherford backscattering spectrometry (RBS). An average number of five ball cratering experiments were carried out in each sample in order to determine its thickness. The morphology of the films was studied by SEM and AFM analyses. Image analysis of images obtained by Optical Microscopy (OM) was also used in order to quantify the superficial defects of the samples, which were determined calculating the ratio between the defective area and the total analyzed area. The superficial roughness of the samples was calculated from 5×5 μm line scans by AFM analyses.

The corrosion behaviour was evaluated by potentiodynamic polarization and electrochemical impedance spectroscopy (EIS) measurements. All electrochemical test were performed at ambient temperature in an artificial sweat solution (pH=4.5), containing 7.5 g l^{-1} NaCl; 1.2 g l^{-1} KCl; 1 g l^{-1} CH_4N_2O (urea) and 1 ml l^{-1} $C_3H_6O_3$ (lactic acid). The electrochemical cell consisted in a standard three electrode arrangement. The counter electrode was a platinum sheet with an area of 1 cm^2 and a saturated calomel electrode (SCE) was used as reference. The area of the working electrode was set in 0.173 cm^2. A PGP201 Potentiostat/Galvanostat (Radiometer Denmark), controlled by the VoltaMaster software, was used to carry out the polarization measurements, while a Voltalab PGZ100 Potentiostat (Radiometer Analytical), controlled by the VoltaMaster-4 software, was used for the EIS measurements. Prior to polarization tests, the open circuit potential (OCP) was monitored during 3600 s, after which the samples were anodically polarized from −800 to 2000 mV at a scan rate of 2 mV s^{-1}. The EIS measurements were performed in the frequency range from 100 kHz to 5 mHz, with an AC sine wave amplitude of 10 mV applied to the electrode at its corrosion potential. EIS measurements were performed at increased immersion times (1, 2 and 3 h, as well as 1, 2 and 3 days). For EIS data simulation, the ZView2 software was used. Previously to corrosion tests, the samples were ultrasonically cleaned in ethanol during 15 min, then in distilled water during 10 min and finally dried. For comparison purposes, a pure Zr film with the same thickness of that of the adhesion layer was used.

3. Results and discussion

3.1. Chemical, morphological and structural characterization

In Table 1, the chemical composition, thickness, superficial roughness and density of defects of the first set of samples (prepared with variation of the bias voltage) are presented. The oxygen fraction in each sample was determined by the ratio between the oxygen content and the sum of both oxygen and nitrogen contents: $fO_2=C_O/(C_O+C_N)$. As it can be seen, the increase in polarization results in a smoother surface, with an increase in the amount of surface defects. The increase of the ion bombardment, resulting from the negative polarization of the growing film, is the main parameter that rules these changes. Moreover,

Table 1
Chemical and morphological characterization of the samples prepared with variation of the bias voltage

Sample	fO_2	Zr (at.%)	N (at.%)	O (at.%)	V_{bias} (V)	Thickness (μm)	R_a (nm)	Defects (%)
$ZrN_{0.81}O_{0.32}$	0.28	47	38	15	0	2.0±0.2	6.2±0.6	1.3
$ZrN_{0.89}O_{0.33}$	0.27	45	40	15	−25	2.5±0.1	5.2±0.5	3.2
$ZrN_{0.90}O_{0.10}$	0.10	50	45	5	−75	2.2±0.2	4.1±0.4	3.6

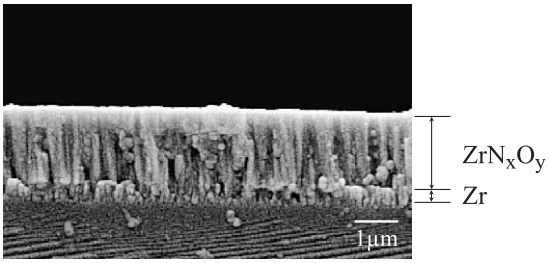

Fig. 1. SEM micrograph of the cross section of a typical sample from the ZrN_xO_y system.

with the increase of this negative bias voltage (increase in the ion bombardment), a reduction of the oxygen fraction in the samples is clearly detected (Table 1). The preferential re-sputtering of oxygen [11], caused by the lower bond strength of the Zr–O in respect to that of Zr–N [12], might be the parameter that can explain this oxygen loss with the increasing bombardment of the growing film.

In Fig. 1, a representative SEM micrograph of the cross section of the films is shown. As it can be observed, the films showed a typical columnar microstructure formed by narrow columnar grains with compactly fibrous morphology. Also, as shown in Fig. 2, the grains present a superficial dome-rounded shape, characteristic of this kind of films [11]. This morphology was also found in the films prepared with the variation of the gas flux (variation of the oxygen fraction).

In Table 2, the chemical composition, thickness, surface roughness and density of defects of the second set of samples, in which the oxygen/nitrogen ratio of the flowing gas was varied, are presented. It is possible to observe lower values of surface roughness for low oxygen fractions, while a higher surface roughness was found to be characteristic of the highest oxygen fractions. In these last samples, an increase in the oxygen fraction also leads to a slight decrease in the roughness, as it can be confirmed by the observation of the AFM images shown in Fig. 2d and e.

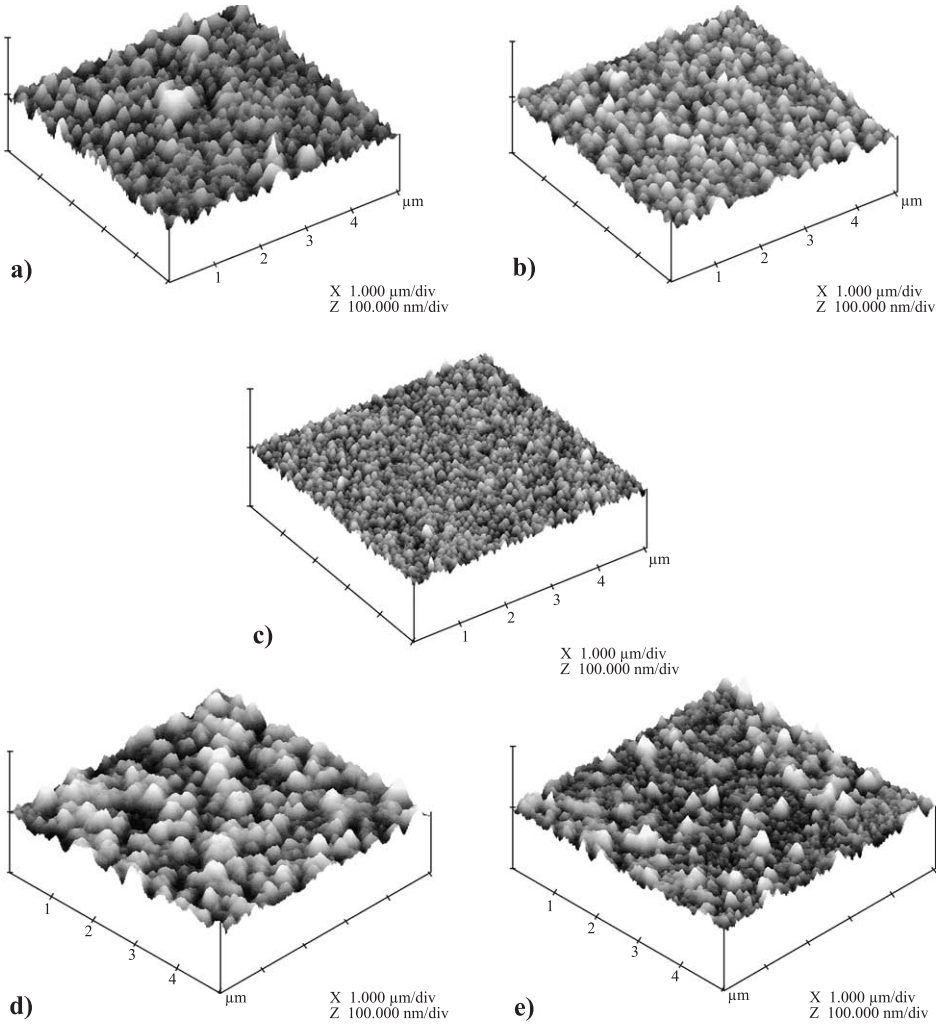

Fig. 2. AFM images showing the morphological changes in ZrN_xO_y thin films. The first two images correspond to samples prepared under different bias voltages: (a) no bias applied and (b) −75 V. The other two images represent changes in samples with different oxygen fractions: (c) $ZrN_{1.14}O_{0.14}$ (f_{O2}=0.11), (d) $ZrN_{0.87}O_{0.30}$ (f_{O2}=0.26) and (e) $ZrN_{0.86}O_{0.41}$ (f_{O2}=0.32).

Table 2
Chemical and morphological characterization of the samples prepared with the same bias voltage (−50 V) and variation of the N/O ratio

Sample	$f O_2$	Zr (at.%)	N (at.%)	O (at.%)	Thickness (μm)	R_a (nm)	Defects (%)
$ZrN_{1.14}O_{0.14}$	0.11	44	50	6	2.3±0.2	3.6±0.4	3.2
$ZrN_{0.91}O_{0.26}$	0.22	46	42	12	3.2±0.1	3.2±0.3	8.4
$ZrN_{0.87}O_{0.30}$	0.26	46	40	14	3.0±0.2	6.0±0.6	7.6
$ZrN_{0.87}O_{0.36}$	0.29	45	39	16	3.2±0.2	5.0±0.5	5.1
$ZrN_{0.86}O_{0.41}$	0.32	44	38	18	1.3±0.1	4.7±0.5	4.3
$ZrNO_{0.50}$	0.33	40	40	20	2.0±0.3	3.6±0.4	3.7

Fig. 3 shows the GIXRD diffraction patterns for representative ZrN_xO_y samples. These films exhibit diffraction patterns corresponding to a fcc ZrN phase. No diffraction peaks from oxide phases were observed. With the growing amount of oxygen, it is admitted that oxygen might be at the grain boundaries and/or within oxide amorphous phases. Furthermore, the ZrN grain size seems to decrease with increasing oxygen fraction and the very broad peak around $2\theta=30^\circ$ is an indication of either the amorphization of the ZrN phase induced by the oxygen inclusion or the formation of an amorphous oxide phase.

3.2. Corrosion behaviour

3.2.1. Influence of the variation of the bias voltage

In Fig. 4a, an overlap of the potentiodynamic polarization curves representative of the behaviour of the samples prepared with the variation of bias voltage is presented. For comparison, the polarization behaviour of the substrate and of a film of pure zirconium is also plotted.

The graph clearly shows that the corrosion resistance of the M2 steel, used as substrate, is clearly enhanced by the deposited films. In contrast, the graph reveals that the pure Zr film, although possessing a lower pitting potential, presents a passive current density one to two decades lower than that of the other films, this being indicative of a superior corrosion resistance. Regarding the oxynitride films, no significant differences between samples are evidenced in Fig. 4a. A well-defined large potential independent region, indicative of a passive plateau, is exhibited by all samples. It should be remarked that a similar behaviour was found for the films prepared with variation of the O/N ratio, which are discussed in the next section. Also, as it can be seen in Fig. 4b, the passive current density for the pure ZrN and ZrO_2 samples is similar to that of the oxynitrides. However, when compared to the other samples, pure ZrN appears to exhibit a slightly lower pitting potential.

In Fig. 5, the evolution of the polarization resistance with the time of immersion in the artificial sweat solution of the films prepared with variation of the bias voltage is

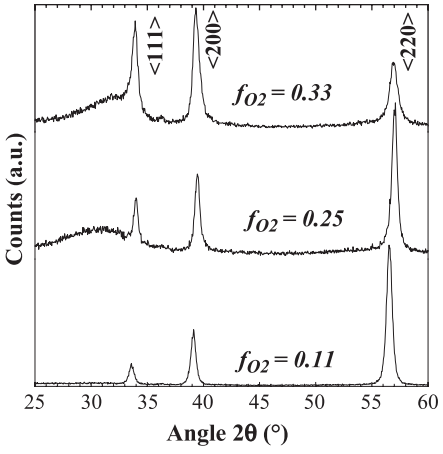

Fig. 3. GIXRD patterns of ZrN_xO_y films with different oxygen fractions.

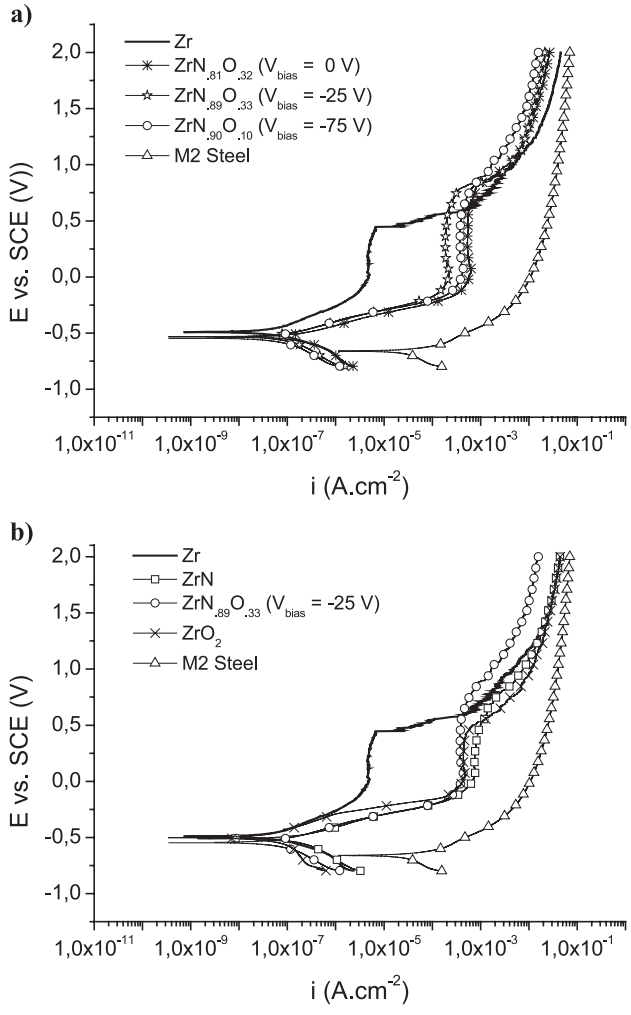

Fig. 4. Anodic polarization curves obtained for ZrN_xO_y prepared with the same N/O ratio and variation of the bias voltage.

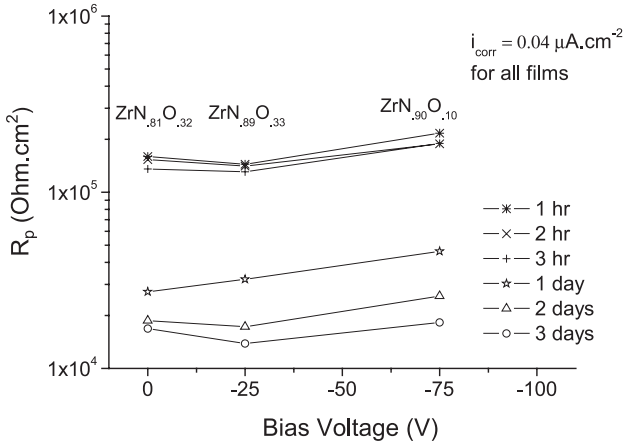

Fig. 5. Influence of the immersion time on the polarization resistance of ZrN_xO_y films obtained at different bias voltages.

presented. It should be referred that polarization resistance is an electrochemical parameter, estimated from the EIS results, which is inversely proportional to the corrosion rate. In fact, from the EIS results an equivalent circuit model is simulated, allowing the substrate polarization resistance (R_{ps}) and the film polarization resistance (R_{pf}) to be deducted. The polarization resistance of the film is then calculated by the sum of R_{ps} and R_{pf}, in accordance to the method described by Liu et al. [13]. A good agreement between the fitted and the experimental data was obtained, as confirmed by the χ^2 values which were always inferior to 1.8×10^{-3}. As it can be observed in Fig. 5, the corrosion resistance of the films appears to be independent of the bias voltage used to process them. Accordingly, as indicated in the figure, the corrosion current density (i_{corr}), calculated from the polarization curves presented in Fig. 4, is low and of the same order of magnitude for all samples. As registered in Table 1, in spite of the increase in the amount of superficial defects when the negative bias voltage is raised, the corrosion resistance of the films remains almost unaltered. It is known that superficial defects can act as preferential routes for the penetration of the solution through the coating [14,15]. However, this mechanism might be compensated by the formation of a more compact structure when negative bias voltage increases, as evidenced by the decrease in surface roughness expressed in Table 1 and Fig. 2a and b. Nevertheless, the protective character of the films tends to diminish with the immersion time, as suggested by the lower values of R_p observed after 3 days of immersion.

3.2.2. Influence of the variation of O/N ratio

Fig. 6 shows the evolution of the polarization resistance as a function of the fO_2. For comparison, in the same curve the i_{corr} values, calculated from the polarization curves, are also presented. The first remark refers to the very low i_{corr} values found for most of the samples. In fact, i_{corr} ranges from values <0.1 μA cm^{-2}, for most samples, up to 0.34 μA cm^{-2} for the film containing a fO_2=0.26. A slight general tendency for an improvement of the corrosion resistance with the increase of the oxygen content can be inferred from i_{corr} and R_p values plotted in the graph, suggesting a superior behaviour of the ZrO_2 film. The behaviour of the pure Zr film should be remarked because it appears to remain a very high R_p even after being in contact with the artificial sweat solution during 3 days. However, in the range $0.22<fO_2<0.33$ the polarization resistance appears to be quite sensitive to small variations of fO_2. Several features, such as the thickness of the film, the density of superficial defects and/or the chemical composition and microstructure of the coatings are expected to influence the corrosion behaviour of these films. From these, microstructure and chemical composition might be considered of prime importance. In fact, comparing, for instances, the behaviour of fO_2=0.26 and fO_2=0.32 films (indicated in Fig. 6), considering the thickness and superficial density of defects of the films presented in Table 2, one can see that in spite of the lower thickness of the fO_2=0.32 film, it presents a better corrosion resistance, perhaps because the fO_2=0.26 film has an higher amount of superficial defects. However, if the comparison is made with the fO_2=0.33, which has slightly less defects and higher thickness than the fO_2=0.32, it will be concluded that the poor corrosion behaviour of the fO_2=0.33 cannot be attributed solely to these parameters. Thus, a complex group of factors are expected to play a role concerning corrosion resistance. Together with variations in chemical composition, grain thinning, texture, amorphization of the ZrN structure, and/or distribution of the oxygen in the structure might also have an important role in this behaviour.

Also, the corrosion resistance of the film appears to be harmfully affected by the time of contact with the solution, as shown in Fig. 7a, which plots the evolution of R_p with the immersion time (for convenience, only one ZrN_xO_y curve—fO_2=0.32—is plotted in the graph). The ZrN film appears to be the most sensitive to this degenerative effect of the film corrosion protection character. On the other hand, the

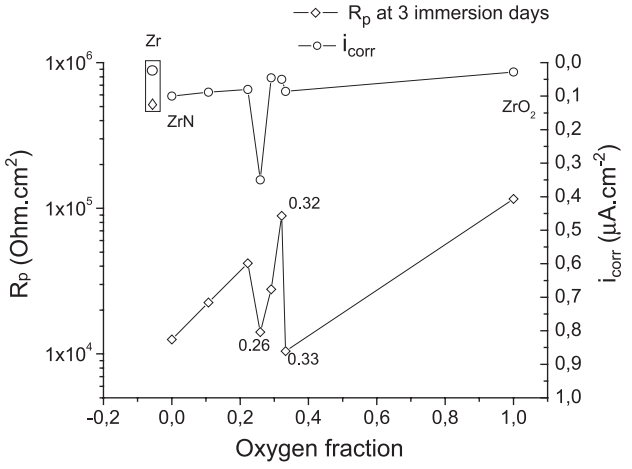

Fig. 6. Influence of the atomic fraction of oxygen on the i_{corr} and polarization resistance (R_p) of the ZrN_xO_y films. For comparison, the i_{corr} and R_p for pure Zr is also plotted.

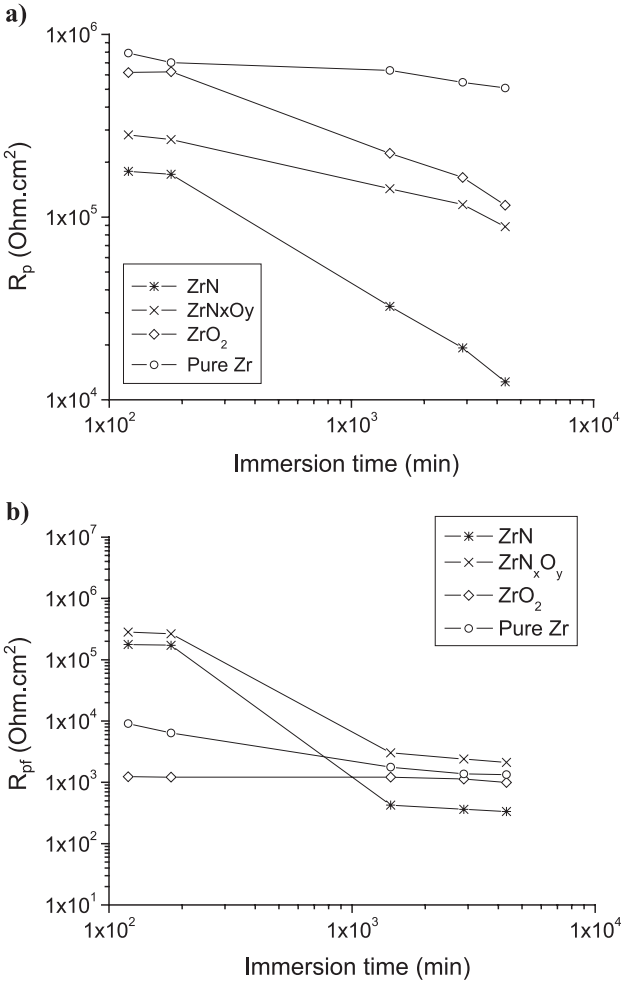

Fig. 7. Evolution of polarization resistance (R_p) (a) and of the film polarization resistance (R_{pf}) (b) with the immersion time in ZrN, ZrN_xO_y, ZrO_2 and pure Zr films.

polarization resistance of the ZrO_2 film approaches that of the Zr film during the first hours of immersion, but then decreases to values near that of the ZrN_xO_y films. In Fig. 7b, the polarization resistance of the film (R_{pf}), estimated from the equivalent circuit models, is plotted [13,15]. This graph allows the behaviour of the film itself to be analyzed independently from the contribution of the substrate. As it can be seen, the values of R_{pf} of the pure Zr film are in close proximity to those of the ZrO_2 film. Also, R_{pf} of both films remains relatively stable throughout the three immersion days, this being an indication of a strong stability of the films when in contact with the artificial sweat solution. In contrast, the protective character of the ZrN and ZrN_xO_y films, although being very high during the first hours of immersion, suffers a strong decrease after 1 day of immersion, showing then a tendency for stabilisation.

The stability of ZrO_2 film may be confirmed by the data presented in Fig. 8a in which the capacitance of the film (C_f) is plotted against the immersion time. In fact, the low capacitance evidenced by the ZrO_2 film when compared to that of the others may be considered as an indication of the superior insulating character of this film. However, as shown in the figure, all films maintain a constant capacitance throughout the immersion time, indicating, as referred above, that other parameters should have influence on the corrosion behaviour. The interdependence of such parameters may be visualised in Fig. 8b which suggests that a relationship between the insulation character of the film (evaluated by C_f) and the density of superficial defects might exist.

The analysis of the Bode plot (frequency vs. phase angle) presented in Fig. 9a and b may also contribute for clarifying the mechanisms involved in the degradation of the films. In fact, coating properties and/or the presence or absence of defects or discontinuities along the different interfaces constituting the coating can be deduced from the observation of the time constants (phase angle maxima) presented in the graph [16–18]. Considering Fig. 9a, which expresses the electrochemical impedance spectroscopic response of the films after 2 h of immersion, two different aspects can be remarked. In first place, with the exception of the ZrO_2 film, all other films show only one time constant, with a high phase angle, in the intermediate to low frequency ranges.

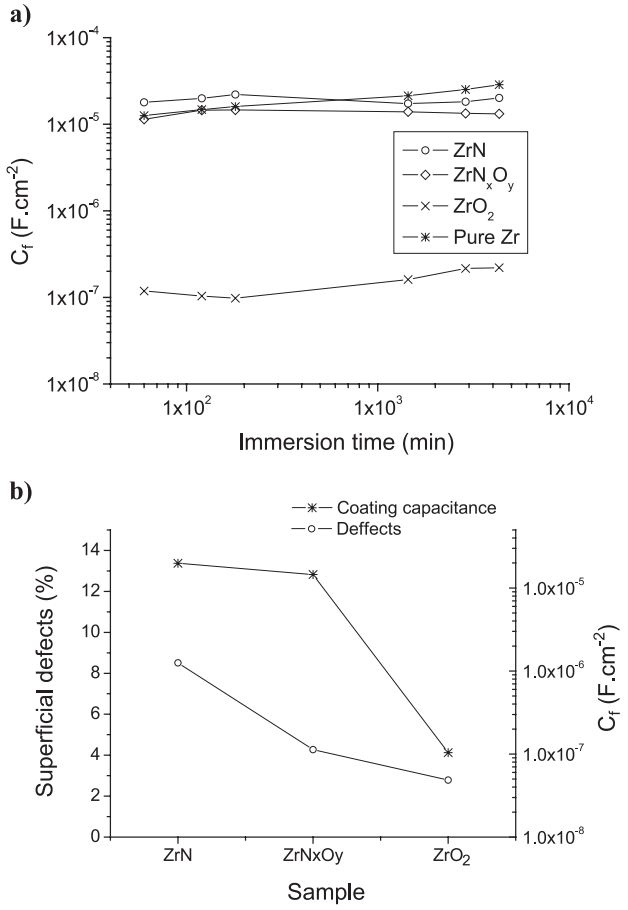

Fig. 8. (a) Evolution of the coating capacitance of the film (C_f) with the immersion time obtained for the ZrN, ZrN_xO_y, ZrO_2 and pure Zr films. (b) Relationship between the film capacitance and the superficial defects for the ZrN, ZrN_xO_y and ZrO_2 films.

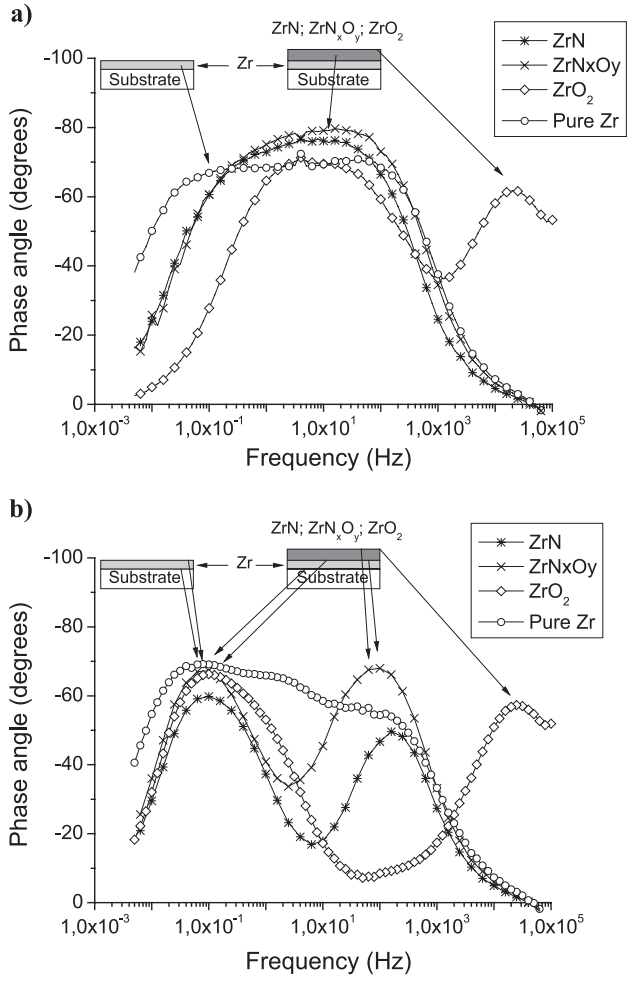

Fig. 9. Bode phase plot (Freq. vs. Phase angle) obtained in ZrN, ZrN_xO_y, ZrO and Zr films after 2 h (a) and 3 days (b) of immersion.

This behaviour is indicative of the good protective characteristics of the film and, eventually, of the system at the film/adhesion layer (Zr) interface level (the solution may possibly penetrate through defects up to the adhesion layer) [16]. Secondly, in the ZrO_2 film the time constant at high frequencies is indicative of a good capacitive behaviour of the solution/film interface, in accordance to the results above referred. It should be stressed that this time constant remains almost unaffected during the immersion time (see Fig. 9b).

However, the Bode plot after 3 days of immersion (Fig. 9b) can provide valuable information regarding the progress of the degradation process of the films. Actually, with the exception of the Zr film, which tends to keep a wide frequency range with a high phase angle, in confirmation of the good response of this film, all other films present now two well-defined time constants. Regarding the ZrN and ZrN_xO_y films, these time constants are located at low and intermediate frequencies. As schematically represented in Fig. 9b, the low frequency time constant might express the substrate/adhesion layer/film interface response, which is better for the pure Zr coating and worst for the ZrN film, in accordance with the results presented above. In the same way, the intermediate time constant might be attributed to the contribution of the adhesion layer/film/solution interface. Again, ZrN films present the worst behaviour. Nevertheless, the ZrO_2 films keep a high value of phase angle at high frequencies, showing a time constant at lower frequencies coincident to the frequency values characteristic of the other films.

4. Conclusions

The corrosion behaviour of ZrN_xO_y films obtained by rf reactive magnetron sputtering was studied. The obtained results allowed the following conclusions to be drawn.

- In the range considered in this work, and in spite of the differences in the chemical and morphological introduced in the samples, the corrosion resistance of the coated steel is not affected by the variation of the bias voltage, if the O/N ratio is kept constant during processing;
- When the O/N ratio is varied during processing, the corrosion resistance tend to be slightly improved by the increase in fO_2;
- However, these improvements are hardly detected by standard potentiodynamic polarization techniques;
- Nevertheless, the corrosion behaviour of the coating system appears to be governed by a complex interrelated ensemble of chemical, structural, textural, morphological and electronic characteristics of the films;
- Pure Zr films show a superior corrosion resistance when compared to the ZrN, ZrN_xO_y and ZrO_2 coating systems. Also, a positive distinctive behaviour of the ZrO_2 films, when compared to the other systems was detected;
- The ZrO_2 film presents an insulator character superior to the other systems. In practice, it appears to possess a higher corrosion resistance than the ZrN and ZrN_xO_y films, due to the cumulative contribution of the good impedance characteristics of the film/solution, film/adhesion layer and adhesion layer/substrate interfaces.

Acknowledgements

The authors gratefully acknowledge the financial support of the FCT Institution by the Contract SFRH/BPD/5518/2001 and by the Project No. POCTI/CTM/380860/2001 co-financed by European community fund FEDER.

References

[1] E. Budke, J. Krempel-Hesse, H. Maidhof, H. Schussler, Surf. Coat. Technol. 112 (1999) 108.
[2] B. Zega, Surf. Coat. Technol. 39/40 (1989) 507.

[3] C. Mitterer, J. Komenda-Stallmaier, P. Losbichler, P. Schmolz, W.S.M. Werner, H. Stori, Vacuum 46 (1995) 1281.
[4] F. Vaz, P. Cerqueira, L. Rebouta, S.M.C. Nascimento, E. Alves, Ph. Goudeau, J.P. Rivière, Surf. Coat. Technol. 174–175 (2003) 197.
[5] F. Vaz, P. Cerqueira, L. Rebouta, S.M.C. Nascimento, E. Alves, Ph. Goudeau, J.P. Rivière, K. Pischow, J. de Rijk, Thin Solid Films 447–448 (2003) 449.
[6] E. Alves, A. Ramos, N. Barradas, F. Vaz, P. Cerqueira, L. Rebouta, U. Kreissig, Surf. Coat. Technol. 180–181 (2004) 372.
[7] M. Bhat, L.K. Han, D. Wristers, J. Yan, D.L. Kwong, J. Fulford, Appl. Phys. Lett. 66 (1995) 1225.
[8] S.V. Hattangady, H. Niimi, G. Lucovsky, Appl. Phys. Lett. 66 (1995) 3495.
[9] W.L. Hill, E.M. Vogel, V. Misra, P.K. McLarty, J.J. Wortman, IEEE Trans. Electron Devices 43 (1996) 15.
[10] R. Fraunchy, Surf. Sci. Rep. 38 (2000) 195.
[11] M. Ohring, The Materials Science of Thin Films, Academic Press, San Diego, 1992.
[12] D. Sherman, D. Brandon, Handbook of Ceramic Hard Materials, Wiley-VCH, New Jersey, 2000.
[13] C. Liu, A. Leyland, Q. Bi, A. Matthews, Surf. Coat. Technol. 141 (2001) 164.
[14] L.A. Rocha, E. Ariza, J. Ferreira, F. Vaz, E. Ribeiro, L. Rebouta, E. Alves, A.R. Ramos, Ph. Goudeau, J.P. Rivière, Surf. Coat. Technol. 180–181 (2004) 158.
[15] C. Liu, Q. Bi, A. Matthews, Corros. Sci. 43 (2001) 1953.
[16] C.H. Tsai, F. Mansfeld, Corrosion 49 (1993) 726.
[17] M.C. Garcia-Alonso, M.L. Escudero, J.L. Gonzalez-Carrasco, J. Chão, Biomaterials 21 (2000) 79.
[18] I. García, J.J. de Damborenea, Corros. Sci. 40 (1998) 1411.